

**Acoustics'08
Paris**
June 29-July 4, 2008

www.acoustics08-paris.org

euonoise

A numerical insight into the effect of confinement on trailing edge noise

Thomas Le Garrec^a, Xavier Gloerfelt^a and Christophe Corre^b

^aArts et Métiers Paris Tech - Sinumef Lab, 151 bd de l'Hopital, 75013 Paris, France

^bLEGI Lab, BP 53, 38041 Grenoble Cedex 9, France

thomas.le-garrec@paris.ensam.fr

The flow and the acoustic field around a 3-D NACA0018 airfoil at Reynolds 1.6×10^5 with an angle of attack of 6° are investigated numerically by direct noise computation. The main purpose of the paper is to study numerically the influence of the confinement due to the walls of the wind tunnel used in the experiments on the flow and acoustic field around the airfoil. The numerical results for a confined airfoil are compared to the results obtained when the top and bottom walls are removed.

1 Introduction

Many experiments used to validate numerical simulations come from results obtained in subsonic wind tunnels which work in closed circuit with a closed test section. These facilities are particularly adapted to phenomenologic studies of complex flows like three-dimensional boundary layers or wakes, flow separations or transition phenomena. The other main used facilities are subsonic wind tunnels which work in open circuit with a free jet. The cross test section of the wind tunnels are sized so that walls have few effects on the flow around the tested body. However, in some configurations, the presence of the walls can influence the aerodynamic and the acoustic fields. One of the first aeroacoustic programme dedicated to the trailing edge noise at high Reynolds number comes from Brooks and Hodgson [1] in 1981. Measurements were conducted in the anechoic quiet-facility at NASA Langley Research center. The airfoil was a NACA0012, with a chord of 609.6 mm and a span of 460 mm. One of the other most studied airfoil is a geometry with an asymmetric 45° beveled trailing edge. This particular trailing edge has been used in theoretical and experimental works, which are summarized in Gershfeld *et al.*[2]. More recently, Shannon *et al.*[3] completed flow field and acoustic investigations on the same airfoil. Influence of an experimental setup has been studied by Moreau *et al.*[4] to make comparisons of their experimental data with simulations in free air. They highlight significant flow field and pressure loading differences, indicating substantial jet interference effects. The studied airfoil had a chord Reynolds number of 1.2×10^5 and was tested in a free jet anechoic wind tunnel. More recently, the french aerospace office ONERA has established a new experimental database [5] named EXAVAC. The test model is a truncated NACA0012 airfoil with a chord length of 495mm. Measurements were carried out in two ONERA's test facilities : the F2 aerodynamic wind tunnel and the CEPRA19 acoustic wind tunnel. Experimental measurements can differ between the two facilities. For instance, in CEPRA19, the angle of attack is modified by a jet deviation phenomenon. A pitch angle correction has been applied to adjust the pressure coefficient to the one obtained in F2.

The direct noise computation (DNC) of the noise generated by the flow over an airfoil is a challenging case. The noise is due to the diffraction of the turbulent structures passing in the vicinity of the trailing edge. So, the turbulent boundary layers, which develop on both sides of the airfoil, have to be discretized enough to capture the fine scales of turbulence. The LES (Large Eddy Simulation) is a good candidate to resolve these fine turbulent scales, without a too fine resolution. The typical resolution requirements for a well-resolved LES in the near-wall region expressed in wall units are approximatively

50 to 100 in the streamwise direction, 10 to 20 in the spanwise direction and 1 to 5 in the normal direction. Even with these values, the LES is still highly expensive for engineering wall bounded flows. An other difficulty of DNC comes from the large disparities between the fine scales of turbulence and the large wavelenghtes of acoustic radiation. So severe constraints on the meshes are imposed in order to include more than one wavelength of the acoustic field in the computational domain. Despite these difficulties inherent to DNC, a growing number of studies attempt to compute directly the airfoil noise in 2-D [6, 7, 8, 9], and recently in 3-D [10, 11, 12]. In the present work, a multi-size-mesh multi-time-step strategy [13, 9] is adopted to limit the number of points and to reduce the calculation cost. The algorithm is briefly presented in the first part. The noise generated by separated-boundary layers over a NACA0018 airfoil at Reynolds 1.6×10^5 is studied in the second part. Effects of the experimental confinement on both flow and acoustic field are highlighted.

2 Numerical algorithm

The three-dimensional compressible Navier-Stokes equations are solved in conservative form on a structured mesh. In the viscous terms, the heat flux terms are modeled by the Fourier law and the shear stress terms are given for a Newtonian fluid. The dynamic viscosity μ is deduced from the Sutherland law. The system of equations is closed with the perfect gaz law. Here, the full 3-D Navier-Stokes equations are solved by using high-order finite differences and an explicit time advancement. A suitable coordinate transform is applied to use curvilinear meshes. The present LES strategy combines a finite-difference scheme with good spectral properties with the use of an explicit filtering without an additional eddy-viscosity model. The effect of SGS motions is taken into account through the regularization induced by the filter.

The main characteristic of our numerical method is that a multi-size mesh multi-time step algorithm is used. It consists in using an adequate local spatial resolution in all the regions of the physical domain. The physical domain is divided in n blocks and if Δx is the smallest scale on the grid, the mesh size of some adjacent block increases by a factor 2. The most important is that there is a corresponding increase in the time step, which allows to relax the severe time step limitation imposed by the explicit time integration. More details are available in ref [9]. The numerical method described in [9] has been extended in three dimensions by using periodic boundary conditions in the spanwise direction. No doubling is imposed in the spanwise direction. In order to reduce the retrieval time, the numerical algorithm is parallelized in the spanwise direction by using the MPI

library.

A third order four-level Adams-Bashforth scheme is used for the time advancement scheme. Two different Adams-Bashforth schemes are used to compute numerical solution at time $(n + 1)$ or $(n + 1/2)$. The numerical solution at time $(n + 1/2)$ is necessary for calculating the interfaces between blocks with a doubling in their mesh sizes. An eleven-point stencil centered finite difference scheme optimized in the wavenumber space [14] is used for spatial derivatives at the interior points. A specific treatment is required at the boundary between two blocks with different mesh sizes. The five points located in the interface of the coarse grid block do not pose any problem by taking every two points from the interface of the finer grid block to keep the interior scheme. On the contrary for the interface of a fine grid block, special stencils are used for the five points near the interface. In the same spirit as ref [15], we choose to keep centered stencils on eleven points, as displayed in figure 1. Coefficients of these eleven-point optimized schemes are reported in ref [9]. An eleven-point centered filter of tenth-order is used for the purpose of removing high-frequency errors and spurious waves due to the use of centered schemes. Filter coefficients for particular points A, B, C, D and E in figure 1 are calculated for the same stencils as the corresponding finite differences.

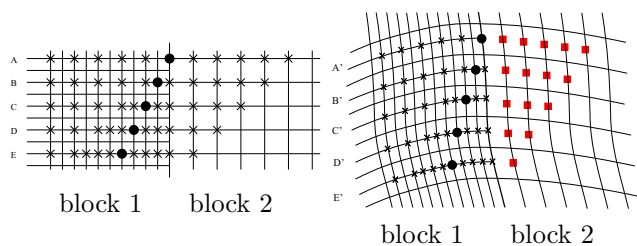


Figure 1: Buffer region between Δx and $2\Delta x$ blocks, and specific centered scheme stencils. (●) application point of the scheme, (×) stencil. Values at points represented by squares (■) must be interpolated.

Furthermore, the finer blocks only receive half of the information needed to compute the next time step. As shown in figure 1, the particular points A', B', C', D' and E' have no counterparts in the coarse grid. So the missing values represented by squares (■) must be interpolated. This operation has to be done in the physical curvilinear space, so that a multi-dimensional interpolation scheme, which takes into account the deformation of the interpolation stencil, is used. The interpolation coefficients are calculated by minimizing an error in the wavenumber space together with some order constraints.

3 Effect of the experimental confinement

The main purpose of this section is to study numerically the influence of the confinement due to the top and bottom walls of the wind tunnel on both the flow and acoustic fields. The main question is: can the experimental results obtained in a wind tunnel with a closed test section be used to validate numerical simulations with no confinement? Generally in CFD, the boundary

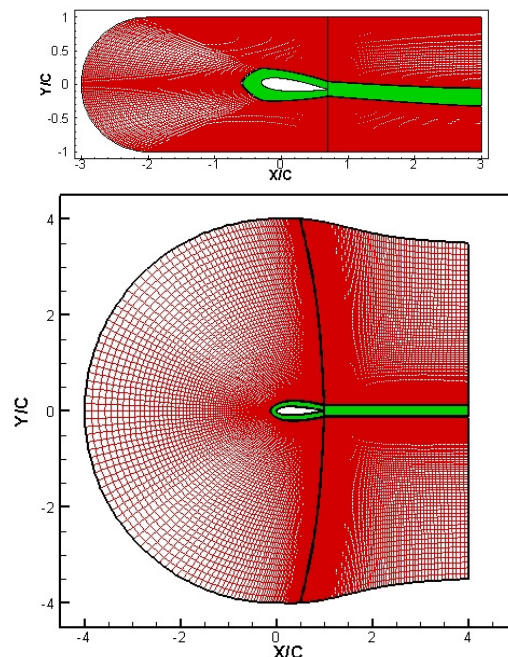
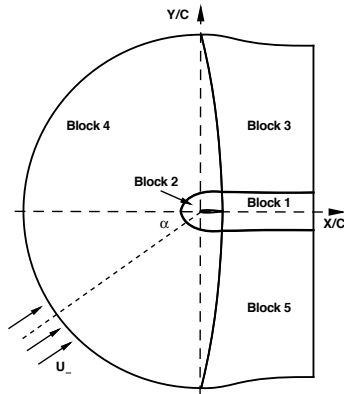


Figure 2: (xy) -cut of the 3-D meshes in the confined (top), and non-confined case (bottom). The color change $0.15C$ away from the airfoil represents the doubling location.

conditions are far away from the airfoil body, so they have no influence on the numerical results. In DNC, the objective is to compute the noise generated by the flow around the airfoil and to propagate it in the overall computational domain. The discretization of the mesh in the far field have to be sufficient to support the acoustic wavelengths. Keeping a reasonable number of points, the boundary conditions are closer from the airfoil body. In order to avoid numerical reflections at the boundary conditions, non-reflecting boundary conditions are used.

3.1 Computational aspects

The flow and the acoustic field around a 3-D NACA 0018 airfoil at Reynolds 1.6×10^5 with an angle of attack α of 6° are investigated numerically by direct noise computation. This configuration matches the experimental setup of Nakano *et al.*[16]. The airfoil has a chord of 80 mm and the section of the wind tunnel is $190 \text{ mm} \times 190 \text{ mm}$. The main difficulty comes from the ability of the code to capture the separation and reattachment points. In order to limit the number of points and to reduce the calculation cost, the multi-size-mesh multi-time-step strategy is adopted. A five blocks configuration is built with one doubling in the radial direction. A 2-D schematic diagram of the mesh is shown in figure 3. The 3-D mesh is obtained by an extrusion in the spanwise direction. Two meshes, shown in figure 2 for both cases (confined and non-confined), are generated. In the confined case, wall boundary conditions are applied on the top and bottom surfaces of the mesh from $X/C = -2$ to 3. The mesh doubling is $0.15C$ away from the airfoil. Parameters of each block are given in table 1. n_ξ , n_η and n_z are the number of points in the circumferential, normal and spanwise directions. The use of the multi-size-mesh multi-time-step algorithm allows to reduce the number of points by a factor 2.33 and 2.48 in the confined and

Figure 3: Sketch of a (xy) -cut of the domain.

non-confined case respectively. The total gain in calculation time, thanks to the possibility to double the time step if there a corresponding increase in the size mesh between two adjacent blocks, reaches more than 3. Each simulation has run for a total of 2×10^6 iterations. The first 10^6 iterations are used to establish the turbulent boundary layer over the airfoil, while the last 10^6 iterations were used to compute the statistics. Each simulation costs approximatively 200 hours on a NEC SX8 supercomputer.

	Confined case	Non-confined case
	$n_x \times n_y \times n_z$	$n_x \times n_y \times n_z$
Block 1	$200 \times 81 \times 41$	$190 \times 81 \times 41$
Block 2	$461 \times 41 \times 41$	$381 \times 41 \times 41$
Block 3	$100 \times 65 \times 41$	$95 \times 95 \times 41$
Block 4	$231 \times 65 \times 41$	$161 \times 95 \times 41$
Block 5	$100 \times 65 \times 41$	$95 \times 95 \times 41$

Table 1: Mesh sizes of the five different blocks making up the computational domain.

3.2 Aerodynamic results

An overall view of the flow around the airfoil is given by the pressure coefficients, $c_p = (\bar{p} - p_\infty) / (0.5\rho_\infty U_\infty^2)$ for both configurations (figure 4). They exhibits significant differences at the leading edge. The positions of the separation and reattachment points are not the same in both cases. The lift and drag coefficients are also significantly modified. In figure 5, the time evolution of lift coefficients indicate an increase by a factor greater than 3 for the confined case. The spectral content is investigated by making power spectral density (PSD) of these signals. In the confined case, a main frequency of 937 Hz is clearly identified in figure 6. This value is very close to the first duct mode, which value is $c_\infty / (2 \times 190 \times 10^{-3}) \approx 911\text{Hz}$. In the non-confined case, the power spectrum shows two principal peaks at 647 Hz and 1558 Hz. The frequency content is more broadband. When the top and bottom surfaces of the wind tunnel are present, a phenomenon of resonance can modify the flow around the airfoil and the structure of the flow, as shown for instance in figure 7 by the visualization of Q criterion, which allows to extract the

coherent structures of the flow.

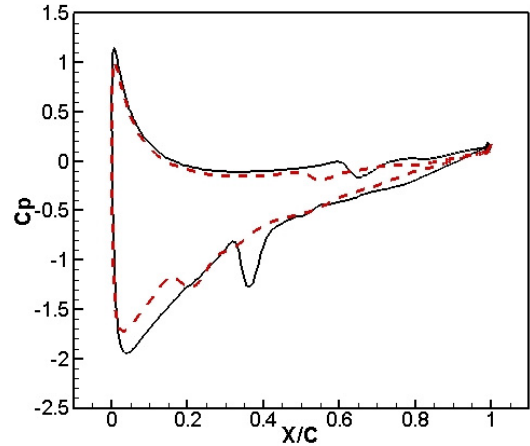


Figure 4: Pressure coefficients on the airfoil with confinement (—) and without confinement (---).

The laminar-turbulent boundary transition is more rapid without confinement than with confinement, suggesting that the blocage effect induces a defavorable pressure gradient, delaying the transition. Another way to analyse the flow around the NACA0018 airfoil is to look at the vorticity field. On the pressure side, the flow is more turbulent in the confined case as shown in figure 8. In the non-confined case, the boundary layer on the pressure side is more attached confirming that the tunnel walls are equivalent to a greater angle of attack. On the suction side, the boundary layer is more separated and ejects some coherent structures when the walls are removed. The flow around the airfoil is thus more asymmetrical. The highly three-dimensional character is clearly visible in the 3-D views of figure 7. PSD of the normal velocity v at two sensors located in the airfoil wake are presented in figure 9. In the confined case, the power spectrum highlights a main frequency at 2500 Hz, whereas in the non-confined the peak is located at 1588 Hz. The signal is more broadband in the latter configuration. On the contrary, the fine peak observed in the confined case, suggest the presence of a more coherent vortex street.

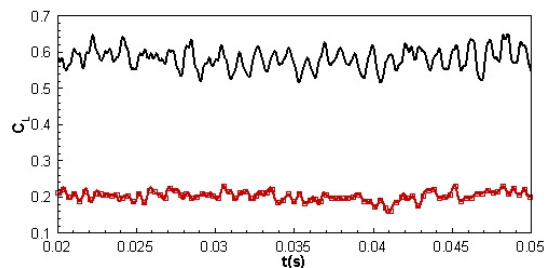


Figure 5: Time evolution of the lift coefficients with confinement (—) and without confinement (---).

3.3 Acoustic results

When the top and bottom surfaces of the wind tunnel are removed, the diffraction of the turbulent structures by the trailing edge generates a broadband power spectrum and the acoustic field has a convected dipolar shape. In figure 10, the 3-D acoustic field is rep-

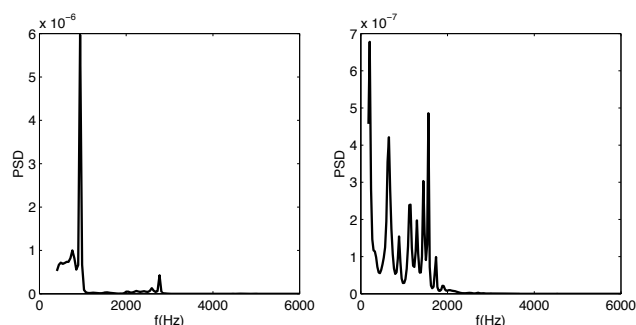


Figure 6: PSD of the lift coefficients for the confined case (left) and non-confined case (right).

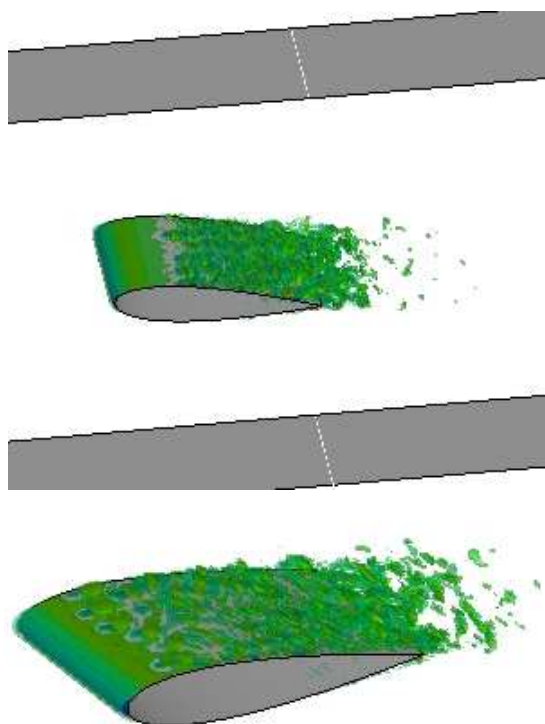


Figure 7: Visualization of the coherent structures by the Q criterion for the confined case (top) and non-confined case (bottom). Contour levels are $\pm 10^8 \text{ s}^{-2}$.

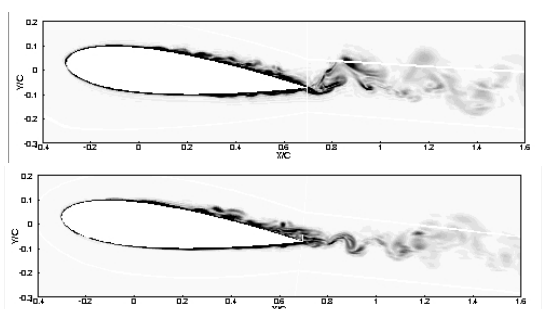


Figure 8: Instantaneous vorticity field $\|\omega\|$ between 0 and $2 \times 10^4 \text{ s}^{-1}$ for the confined case (top), and the non-confined case (bottom).

represented in the overall computational domain. Three-dimensional effects are clearly visible on the acoustic field, which bears a modulation in the spanwise direction. A cut in the median plane is plotted in figure 11. The principal wavelength is shown to vary in time. In the confined case, the acoustic field is typical of resonance as depicted in figure 11. The sound generated by the flow around the NACA0018 airfoil excites the first duct mode and lays into resonance. These results are confirmed by the study of some acoustic sensors located at $\Theta = (90^\circ, 135^\circ, 180^\circ, 225^\circ, 270^\circ)$ and $R = 1C$ (confined case) or $R = 3.75C$ (non-confined case). The origin is fixed at $(X/C, Y/C) = (1, 0)$ and the angles Θ are measured in the anti-clockwise direction from the horizontal axis. The noise is lower at $\Theta = 180^\circ$ than at $\Theta = 90^\circ$ because the sensor is placed in the silent zone. The PSD's displayed in figure 12 highlight a primary discrete peak at a frequency of 1545 Hz, which is very close to the main vortex street frequency (1588 Hz) and to the fluctuating lift frequency (1558 Hz). So, the acoustic field can be directly linked to the vortex street which develops in the airfoil wake. In the confined case, the main frequency (952 Hz) is very close to the first duct mode and the pressure levels are severely increased by the resonance (about $\pm 20 \text{ Pa}$ in the confined case, and $\pm 2 \text{ Pa}$ in the non-confined case). This frequency is close to that of the lift fluctuations. The pressure field on the airfoil is therefore dominated by the acoustic resonance.

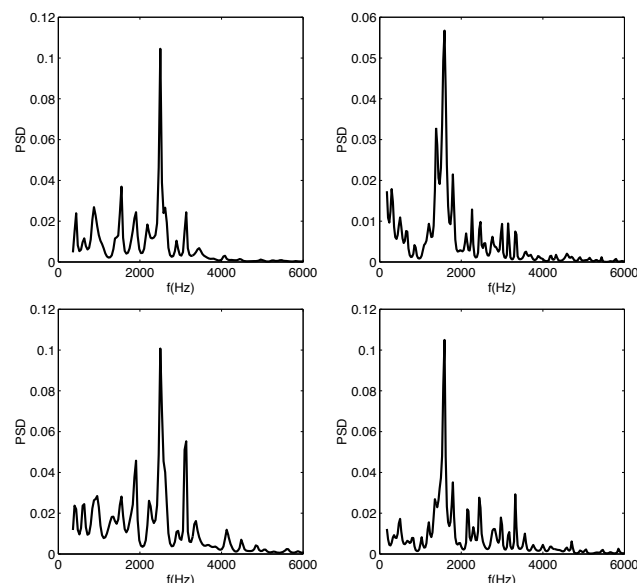


Figure 9: PSD of the normal velocity sensors at $X/C = 1.02$ (top) and $X/C = 1.08$ (bottom). Left: confined case. Right: non-confined case.

3.4 Conclusion

Effects of the experimental confinement have been clearly demonstrated by running two numerical simulations over a NACA0018 airfoil with or without the top and bottom walls of the wind tunnel. Therefore, making a numerical simulation of the NACA0018 airfoil in the same conditions as the experiments of Nakano *et al.*[16] is quite difficult. Indeed, in their experiments, the top and bottom

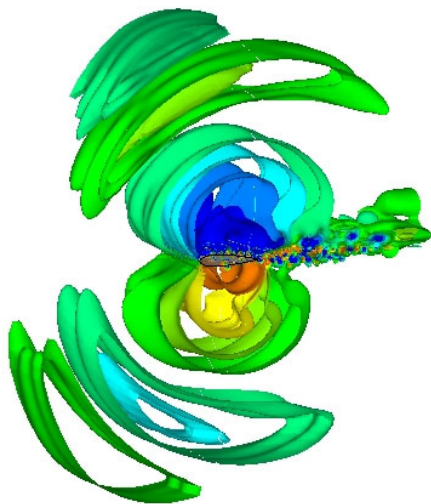


Figure 10: 3-D view of the acoustic field in the non-confined case, ± 3 Pa.

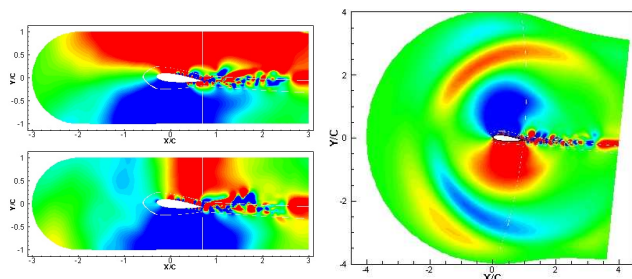


Figure 11: 2-D views in the median plane of the acoustic field for the confined case (left), ± 10 Pa and the non-confined case (right), ± 5 Pa.

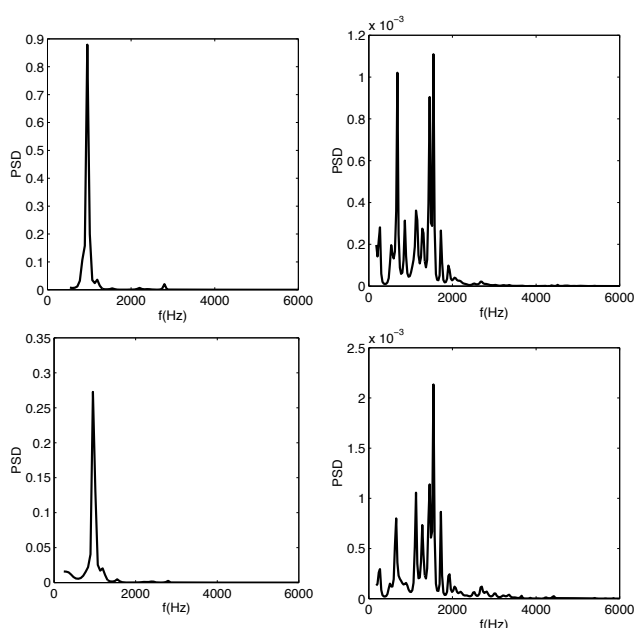


Figure 12: PSD of fluctuating pressure at $\Theta = 90^\circ$ (top) and 135° (bottom). On the left: confined case. On the right: non-confined case.

of the test section were made of wood-glass material of 25 mm thickness to remove the acoustic resonance, while the side planes were transparent for the flow visualization. Even with the use of wood-glass material, Nakano *et al.* detected a small peak in the sound spectra caused by the resonance between the airfoil and the wind tunnel walls. Numerically, the wood-glass material should be represented by an impedance boundary condition which mimics the effect of a sound absorbing liner. Numerical implementation of such a condition was out of the scope of the present work. To conclude, when the wind tunnel walls of a closed test section are close to the airfoil body, the experimental measures have to be used with caution to validate a numerical simulation without any confinement.

Acknowledgments

Supercomputer time supplied by Institut du Développement et des Ressources en Informatique Scientifique (IDRIS - CNRS) made these computations possible. The authors thank the DGA (Direction Générale de l'Armement) for its support.

References

- [1] BROOKS, T.F. & HODGSON, T.H., 1981, Trailing edge noise prediction from measured surface pressures, *J. Sound Vib.*, **78**(1), p. 69–117.
- [2] GERSHFELD, J.L., BLAKE, W.K. & KNISELY, C.W., 1988, Trailing edge flow and aerodynamic sound, *AIAA Thermophysics, Plasmadynamics and Lasers Conference, San Antonio, Texas* AIAA Paper 1988-3826, p. 2133–2140.
- [3] SHANNON, D.W., MORRIS, S.C. & MUELLER, T.J., 2006, Radiated noise and turbulent motions in a blunt trailing edge flow field, *Heat and Fluid Flow*, **27**(4), p. 730–736.
- [4] MOREAU, S., HENNER, M., IACCARINO, G., WANG, M. & ROGER, M., 2003, Analysis of flow conditions in freejet experiments for studying airfoil self-noise, *AIAA Journal*, **41**(10), p. 1895–1905.
- [5] BULTÉ, J., DAVY, R. & MANOHA, E., 2007, Airfoil noise and unsteady flow measurements for the validation of cfd/caa methods, *AIAA Paper 2007-3454*.
- [6] TAM, C.K.W. & JU, H., 2006, Numerical simulation of the generation of airfoil tones at a moderate reynolds number, *AIAA Paper 2006-2502*.
- [7] HATAKEYAMA, N. & INOUE, O., 2006, Direct numerical simulation of noise from an airfoil in a uniform flow, *AIAA Paper 2006-2504*.
- [8] DESQUESNES, G., TERRACOL, M. & SAGAUT, P., 2007, Numerical investigation of the tone noise mechanism over a laminar airfoil, *J. Fluid Mech.*, **591**, p. 155–182.
- [9] LE GARREC, T., GLOERFELT, X. & CORRE, C., 2007, Multi-size-mesh, multi-time-step algorithm for noise computation around an airfoil in curvilinear meshes, *13th AIAA/CEAS AeroAcoustics Conference*, 21-23 May, Roma, Italy, AIAA Paper 2007-3504.
- [10] MARSDEN, O., BOGEY, C. & BAILLY, C., 2008, Direct noise computation around a turbulent flow around a zero-incidence airfoil, *AIAA Journal*, **46**(4), p. 874–883.
- [11] SANDBERG, R.D., JONES, L.E. & SANDHAM, N.D., 2008, Direct numerical simulations of noise generated by turbulent flow over airfoils, *AIAA Paper 2008-2861*.
- [12] LE GARREC, T., GLOERFELT, X. & CORRE, C., 2008, Direct noise computation of trailing edge noise at high reynolds numbers, *14th AIAA/CEAS AeroAcoustics Conference*, 5-7 May, Vancouver, Canada, AIAA Paper 2008-2914.
- [13] TAM, C.K.W. & KURBATSKII, K.A., 2003, Multi-size mesh multi-time-step dispersion-relation-preserving scheme for multi-scales aeroacoustics problems, *International Journal of Computational Fluid Dynamics*, **17**, p. 119–132.
- [14] BOGEY, C. & BAILLY, C., 2004, A family of low dispersive and low dissipative explicit schemes for noise computation, *J. Comput. Phys.*, **194**, p. 194–214.
- [15] TAM, C.K.W. & KURBATSKII, K.A., 2000, Micro-fluid dynamics and acoustics of resonant liners, *AIAA Journal*, **38**(8), p. 1331–1339.
- [16] NAKANO, T., FUJISAWA, N., OGUMA, Y., TAKAGI, Y. & LEE, S., 2006, Experimental study on flow and noise characteristics of NACA0018 airfoil, *J. Wind Eng. Ind. Aerodyn.*